Instruments and Methods

A non-destructive method for measuring the salinity and solid fraction of growing sea ice in situ

Dirk NOTZ,[1*] John S. WETTLAUFER,[2] M. Grae WORSTER[1]

[1]*Institute of Theoretical Geophysics, Department of Applied Mathematics and Theoretical Physics, University of Cambridge, Wilberforce Road, Cambridge CB3 0WA, UK*
E-mail: dn240@cam.ac.uk
[2]*Department of Geology & Geophysics and Department of Physics, Yale University, New Haven, Connecticut 06520-8109, USA*

ABSTRACT. We describe an instrument developed to make in situ measurements of salinity and solid-fraction profiles in growing sea ice. The vertical resolution of the measurements is up to a few millimeters, with a temporal resolution of up to fractions of a second. The technique is based on impedance measurements between platinum wires around which sea ice grows. Data obtained using this instrument in laboratory experiments are in good agreement with theoretical predictions. In a field test in the Arctic, the bulk salinity of growing sea ice has been measured in situ throughout the whole depth of the ice layer. The data are compared with bulk salinities obtained from ice cores, and confirm the general understanding that the bulk salinity in ice-core studies is significantly underestimated in the lower parts of the cores. The approach can also be used in other glaciological applications and for general studies of two-phase, two-component porous media.

1. INTRODUCTION

During the growth of sea ice, salt cannot be incorporated into the ice crystals themselves, so is either rejected into the underlying ocean or remains within highly saline brine in the interstices between the pure, fresh-water ice crystals. It is the volume fraction of this brine, the so-called liquid fraction, which determines some of the main properties of sea ice and its interaction with the environment: the heat capacity and conductivity of sea ice are strong functions of its liquid fraction, as are its mechanical and electromagnetic properties (Schwerdtfeger, 1963; Weeks and Assur, 1967; Ono, 1975; Morey and others, 1984); the salt rejected from the ice influences the vertical stratification of the ocean and thereby plays an important role in the global thermohaline circulation (Aagaard and others, 1981; Carmack, 2000); and the latent heat that is released when a certain volume of sea ice is completely melted is proportional to the solid fraction. Knowledge of the liquid and solid fractions of sea ice is therefore essential for adequately modelling its growth and decay.

Whereas theoretical estimates of the salinity distribution of perennial ice are in good agreement with measurements (Schwarzacher, 1959; Untersteiner, 1968), the salinity evolution of first-year ice is still only poorly understood. It is the small areal fraction of first-year ice that dominates the wintertime heat balance and negative oceanic buoyancy forcing in polar regions. Field and laboratory studies of the evolving phase fraction of first-year ice, which controls its bulk behaviour, differ from the specified properties used in large-scale numerical models (Wettlaufer and others, 2000). A first-principles predictive model of the brine volume evolution is therefore required in order to understand the relationship between seasonal freezing, especially in shelf regions and shallow seas, and thermohaline circulation. To provide reliable tests for such a model, accurate and extensive measurements of salinity in growing sea ice are required.

In this paper, we introduce an instrument that is able to measure the liquid fraction and the salinity of newly formed sea ice in situ. The technique, which relies on the measurement of electrical impedance, can be used in a fully automated stand-alone configuration and allows for nearly any desired spatial and temporal resolution. It is described and compared with other methods of measuring brine content in section 2. In section 3 the data analysis and the results of measurements of solid-fraction and bulk salinity for a simple laboratory experiment with constant cooling from below are presented and compared with theoretical predictions. Section 4 contains data from a field experiment on Svalbard, in which the instrument was used for a period of 9 days to measure the solid fraction and the bulk salinity of growing sea ice. In section 5 we discuss other possible applications of the instrument.

2. MEASUREMENT OF SEA-ICE SALINITY

Measurement of the temporal and spatial evolution of the salinity profile in sea ice has been a common part of Arctic and Antarctic field campaigns since the beginning of scientific polar exploration and of many laboratory experiments (Malmgren, 1927; Weeks and Lee, 1958; Schwarzacher, 1959; Cox and Weeks, 1975; Nakawo and Sinha, 1981; Cottier and others, 1999; Perovich and others, 1999). In addition to the usual method of taking ice cores, two other techniques have been used; radioactive tracers (Cox and Weeks, 1975) and time-domain reflectometry (TDR)/capacitance measurements (Morey and others, 1984; personal
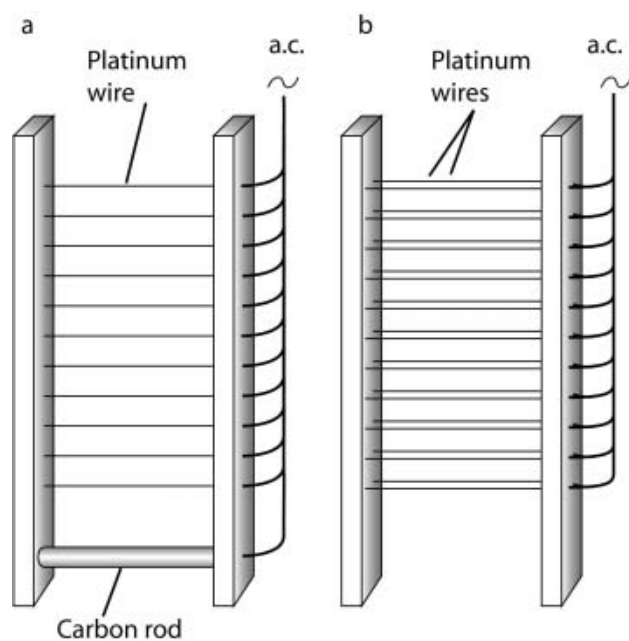
Fig. 1. (a) Sketch of the instrument used by Shirtcliffe and others (1991), in which the impedance was measured between individual wires and a carbon rod. (b) Sketch of the improved instrument, in which the impedance is measured between two wires at each level.

communication from L. Bäckström and H. Eicken, 2004). Here we introduce a new technique based on measurements of electrical impedance. Each of these techniques has certain advantages and disadvantages, which are summarized in this section.

2.1. Coring method

By far the most widespread and easily applicable method for measuring sea-ice salinity is by direct measurement of ice cores. Varying barrel sizes and designs are used to remove sections and sample sea ice. The strength of the approach is simplicity. The principal drawback is brine drainage driven by the removal of the sample from hydrostatic equilibrium. The method is destructive and hence incapable of observing rapid temporally varying salinity profiles in situ. Long continuous time series spanning a couple of weeks are seldom measured, as the drilling process cannot easily be automated.

2.2. Radioactive tracers

In a laboratory experiment, Cox and Weeks (1975) grew ice from a radioactive sodium-chloride solution and measured the space–time evolution of the salinity distribution. The method achieves a 1 cm spatial resolution and resolves profiles on 1–16 hour time-scales. It is not amenable to use in the field.

2.3. Time-domain spectroscopy and capacitance measurements

TDR is a technique used to estimate the liquid fraction in a host of partially frozen systems (e.g. Arcone and Wills, 1986). It exploits the fact that in the frequency range between 50 MHz and 1 GHz the dielectric properties of ice and water differ substantially, but are only weakly frequency-dependent. The reflection and absorption of electromagnetic waves through a sample can be analyzed

to determine the liquid fraction. In combination with measurements of the vertical temperature profile, the salinity profile can be determined with cm resolution (Morey and others, 1984; Campbell, 1990; personal communication from L. Bäckström and H. Eicken, 2004).

2.4. Impedance measurements

The technique that we present in this paper allows the in situ measurement of the temporal and spatial evolution of the salinity and solid-fraction distribution in newly forming mushy layers, which in general are two-phase, two-component reactive porous media, of which sea ice is an example. The technique is non-destructive, offers very high spatial and temporal resolution and can be used fully automated as a stand-alone, battery-powered system. Its main drawback, especially compared to TDR and capacitance measurement techniques, is that it cannot measure the salinity distribution in pre-existing mushy layers but must be deployed in a liquid (e.g. open sea water). The instrument described here is based on that developed by Shirtcliffe and others (1991), hereafter referred to as SHW. Their instrument measured the impedance between individual thin horizontal platinum wires frozen into the mush, and a large carbon electrode immersed in the underlying liquid (Fig. 1a). Because pure ice is a good electrical insulator, the measured impedance is a strong function of the volume fraction of ice crystals. Therefore the impedance measured at different wires can be used to calculate the profile of the solid fraction. At the level of each wire the temperature is also measured, so that the salinity of the interstitial brine can be inferred from the liquidus relationship. The bulk salinity is obtained by multiplying the solid fraction and the local brine salinity. Such an instrument has been used to obtain results in good agreement with theoretical predictions for laboratory experiments of solidification of $NaNO_3$ without gravitational effects (SHW; Chiareli and Worster, 1992). Initial trials of such an instrument in the field on Svalbard (February 2001 and March 2002) showed a clear signal and an expected increase in solid fraction with time and decrease with depth. However, a detailed analysis suggested that the measurements were compromised by brine draining from the sea ice affecting the electrical environment of the carbon electrode and by ocean currents affecting ionic charge transport.

We have therefore developed an instrument in which the impedance is not measured between single wires and a carbon block but between pairs of wires closely spaced horizontally (see Fig. 1b). Such a set-up had previously been used by Shirtcliffe and Kerr (1992), who reported that the data were too difficult to interpret. However, we have found no difficulty in analyzing the data from this type of instrument, and obtain good agreement with the single-wire measurements.

The major assumption in extracting the solid fraction from the impedance measurement is that the measured impedance between each pair of wires is proportional to the fraction of the wire that is surrounded by ice. To average out inhomogeneities of the brine distribution in sea ice, the wires should be significantly longer than the typical grain-size of a few centimetres. The instrument that we used consists of 14 pairs of platinum wires, each wire having a length of 120 mm. The diameter of the wires should be chosen as small as possible to minimize the impact of the instrument on the natural ice growth. We use wires with a

diameter of 0.25 mm. To find the ideal horizontal spacing between the two wires in each pair, we carried out a series of sensitivity studies and found that for frequencies below 5 kHz the measured impedance does not change significantly for a horizontal spacing between 1 and at least 13 mm, which was the maximum spacing mechanically obtainable from the instrument used for this specific test. We chose a horizontal spacing of 5 mm, mostly for mechanical reasons. The vertical spacing between the wire pairs in our instrument varies from 5 to 25 mm, with the smaller spacing at the top of the instrument to obtain a higher resolution for the initial stages of sea-ice formation. The 5 mm minimum spacing used in our instrument was again chosen for mechanical reasons. This spacing can be freely adjusted according to the intended application and could for example be tens of centimetres for studies of multi-year ice. The thermistors, which measure the vertical temperature distribution in the ice as it forms, are directly attached to the instrument to allow easy deployment in the field.

As SHW point out, the presence of the wire in the supercooled liquid just ahead of a growing crystal might act as a nucleation site and change the morphology of the forming ice. However, neither visual inspection nor the comparison of measured data with theoretical predictions indicated any significant impact of the wire on the growing ice. To prevent heat transfer from the insulated copper wires that connect the platinum wires to the electronics package, these wires are mounted such that they run horizontally for a few centimetres before being attached to the platinum wires.

The electronics package consists of a signal generator, an amplifier and a datalogger, as depicted schematically in Figure 2. The voltage drop V_S of the sinusoidal input signal over a reference resistor and the voltage drop V over each of the platinum-wire pairs are measured and logged by the datalogger. To obtain a steady reading with a high resolution, both V and V_S are filtered, rectified and amplified before being measured. From the two voltages, the impedance Z of the measurement volume, i.e. of the sea ice in our case, can be calculated by using $|V| = Z \cdot |I|$ and $|V_S| = R_S \cdot |I|$. Here, I is the current through the system, the measurement of which could also be used in the determination of Z. We use a multiplexer consisting of an MC14514B multiplexer chip which connects one wire pair after the other to the signal generator by controlling a bank of 16 relays. The MC14514B itself is controlled by a DataTaker 800, which can be programmed to switch individual digital channels.

Our signal generator consists of an ICL8038 chip that, even though only certified for a temperature range above 0°C, works well at least down to a temperature of −30°C. We use a 2 kHz sinusoidal signal that is amplified by a UA741 amplifier before being transmitted to the platinum wires. To minimize errors in the impedance measurements, introduced by the connections between the instrument itself and the electronics, we use low-impedance cables. Both the multiplexer with the relays and the signal generator are mounted onto a single PCB board to minimize the connection lengths between the individual components.

For the temperature measurement we use Yellow Springs YSI44035 thermistors which are connected directly to the input channels of the DataTaker 800. The whole system is battery-powered and is automatically switched off outside measurement periods with a power consumption of <1 mW when in 'sleep mode'.
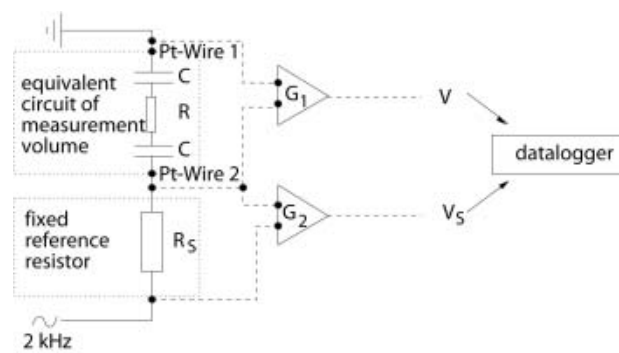

Fig. 2. Circuit used to measure the impedance between the two wires of an individual wire pair. G_1 and G_2 are filters, rectifiers and amplifiers, C is a capacitor and R is a resistor. V and V_S are d.c. voltages the ratio of which is used to determine the impedance of the measurement volume.

3. DATA ANALYSIS AND LABORATORY EXPERIMENT

In this section, we present data obtained in simple laboratory experiments to explain the procedure by which the physically relevant parameters (solid fraction and bulk salinity) can be derived from the directly measured parameters (impedance and temperature), and to test the underlying assumptions against theoretical predictions.

In the first experiment, a 35 ppt (parts per thousand) NaCl solution with an initial temperature of +6°C was cooled from below in a thermally insulated tank, with the base temperature held constant at −20°C. The liquidus temperature of this solution, i.e. the temperature at which a solid phase occurs at a certain concentration, can be calculated from the liquidus relationship for NaCl solutions

$$T_1 = (-5.33 \times 10^{-7} S^3) - (9.37 \times 10^{-6} S^2) - 0.0592 S, \quad (1)$$

where S is the NaCl concentration in ppt and T_1 is in °C. Equation (1) has been derived from a cubic fit to the experimental data in Weast (1971). For concentrations below $S = 40$ ppt the linear fit $T_1 = -0.0598 S$ is accurate to within 1%.

For the 35 ppt NaCl solution that we use, $T_1 = -2.10$ °C. From the measurements of impedance $Z(t)$ and temperature $T(t)$ as functions of time at the wire pair 2.5 cm above the bottom of the tank, we plot the impedance as a function of temperature in Figure 3. Note that while the figure is qualitatively independent of the solution used, it is quantitatively only valid for this particular set-up. While the temperature at the level of the wires decreased from +5 °C to the local freezing point, the impedance increased slowly due to the increasing viscosity of the water and the accompanying reduction in ion mobility and therefore lower electrical conductivity. Once the freezing point of the solution was reached, the impedance increased much faster with decreasing temperature as more of the wires was electrically insulated by the growing ice. It is this strong dependence of the impedance on the solid fraction of the ice surrounding the wires that forms the basis of our measurement technique.

By taking the ratio of the impedance Z_0 when ice starts to form and the impedance Z at a lower temperature, a rough estimate of the liquid fraction can be obtained. For a more accurate estimate, the change of the conductivity of the
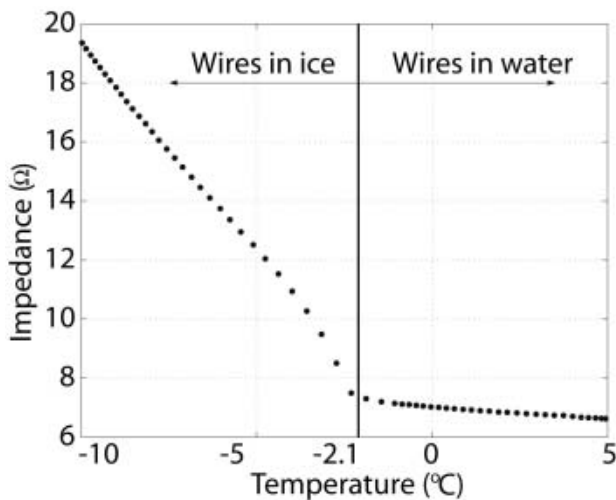
Fig. 3. Impedance as a function of temperature as measured at the wire pair 2.5 cm above the bottom of a tank in which a 35 ppt NaCl solution is cooled from below. Note that in such a set-up no brine drainage occurs and the measured impedance is significantly lower than would be found in low-saline sea ice.

Fig. 4. A comparison of the solid fraction as measured between the wires of a single wire pair and between each of the two wires and a carbon rod immersed in the solution. Data from an experiment in which a 5.6% NaNO$_3$ solution was cooled from below to $-14\,°C$. The two wires, which were located 8 mm above the bottom of the tank, were separated from each other by a horizontal spacing of 5 mm and were situated 30 cm below the carbon rod.

interstitial brine with salt concentration and temperature must be taken into account. Thus, if the conductivity of the interstitial brine is γ, the conductivity of the brine when ice formation started is γ_0 and ϕ is solid fraction, the liquid fraction $(1 - \phi)$ can be calculated from the relationship

$$1 - \phi = \frac{\gamma_0 Z_0}{\gamma(T, S)Z}, \tag{2}$$

as given by SHW. Here T is the temperature that has been measured at the same depth as the impedance, and S is the brine concentration at that level as calculated from the liquidus relationship Equation (1), which can be inverted to give

$$S = -0.00361 T^3 - 0.388 T^2 - 17.6 T. \tag{3}$$

The main difficulty lies in accurately determining the functional form of γ as a function of salinity and temperature. In order to do so, a basic knowledge of the way a conductivity cell works is essential (Bard and Faulkner, 1980; Atkins, 1998). In the configuration that we use, with a sinusoidal frequency of 2 kHz, an amplitude of 1 V and low-impedance connections to the platinum wires, the equivalent circuit for a wire pair can simply be thought of as being a series of a capacitor and a resistor (Daum and Nelson, 1973). The capacitance is caused by the formation of electrical double layers (e.g. Hunter, 2001) directly surrounding the wires, and the resistance is caused by the limited conductivity of the liquid between the two wires. An *electrical double layer* forms when a charged surface is brought into contact with an electrolyte solution. It consists of the charge of the electrode and an equal and opposite charge of the ions in the solution that accumulate close to the electrode. Using Debye–Hückel theory, it can be shown that the typical length scale of the electrical double layer for sea water is several nanometres. Whenever an alternating current is applied to such a double layer, the double layer acts as a capacitor. In our set-up the impedance formed by the electrical double layers dominates the resistance between the wires, which is why the impedance does not change with changing horizontal spacing of the wires as was found in the sensitivity study (see section 2.4). Hence,
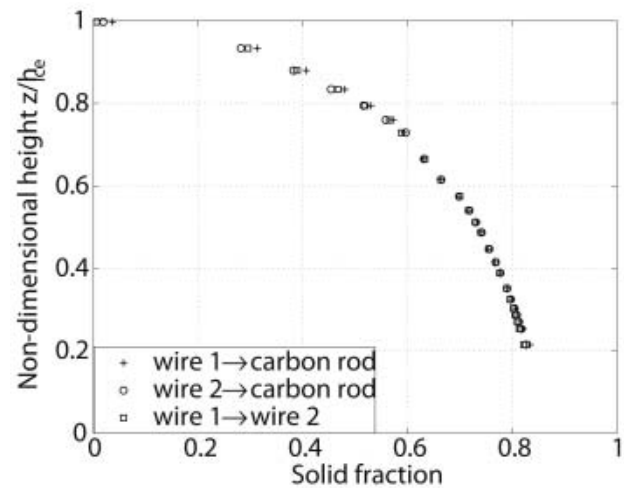
the impact of the geometrical distribution of the ice between the wires that is for example taken into account in the analysis by Chiareli and Worster (1992) can be neglected. The total impedance of the series of the capacitor C_d of the double layer and the resistance R of the fluid between the wires is

$$Z = \left(\frac{1}{(2\pi f C_d)^2} + R^2\right)^{1/2}. \tag{4}$$

As derived in Hunter (2001) for example, the capacitance of the electrical double layer can be described as $C_d = A\sqrt{S}$, where A is a function of the geometrical properties of the conductivity cell, the temperature and the physical and chemical properties of the solution to be measured. For a certain chemical composition of the solution, a change in the concentration does not affect the value of A, which can therefore be treated as constant at constant temperatures for a given experimental set-up. The resistance between the wires is almost negligible, and hence the functional form of the conductivity at a fixed temperature γ_{20} is

$$\gamma_{20}(S) = BS^{1/2}, \tag{5}$$

where B is a constant. This equation has been obtained by using the fact that the impedance of a capacitance is $Z_C = 1/(2\pi f C_d)$ and the conductivity is proportional to $1/Z$.

However, with our electronics we find a power-law fit according to

$$\gamma_{20}(S) = 0.05 S^{0.33}, \tag{6}$$

at $T = 20°C$, where the different exponent (cf. Equation (5)) is probably caused by the influence of the finite resistance between the wires. For the range of temperatures and concentrations that are of interest in the solidification of NaCl solutions corresponding to sea water, we find a temperature dependence described by the simple relationship

$$\gamma = \gamma_{20} - 0.0015 \Delta T. \tag{7}$$

Here ΔT is the temperature deficit below $20\,°C$, S is in ppt
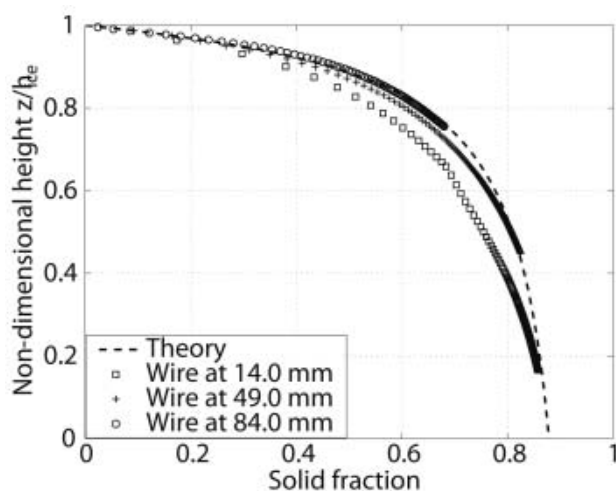
Fig. 5. A comparison of the measured and the theoretically predicted solid fraction. The data stem from wires in different heights in a tank in which a 35 ppt NaCl solution is cooled from below to −20 °C.
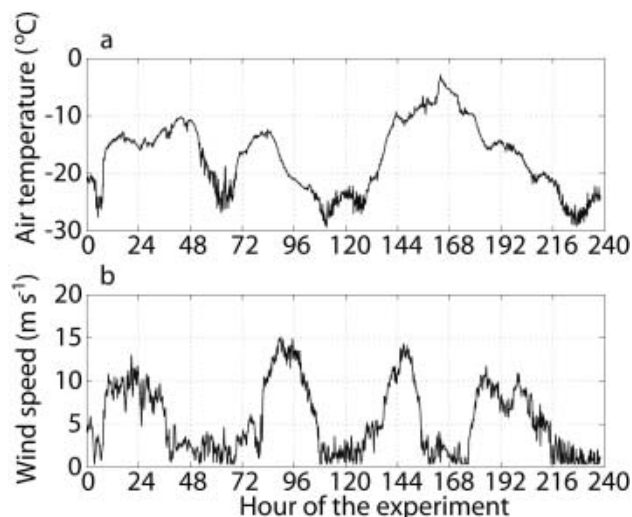

Fig. 6. Temperature (a) and wind (b) data from the weather station in Adventdalen, Svalbard, for the duration of the experiment on Adventfjord. The weather station is located 4 km from the site of the experiment.

and γ is obtained in $\Omega^{-1}\mathrm{m}^{-1}$. Both Equations (6) and (7) were obtained from a series of experiments in which the impedance was measured for salt solutions with salinities of 10–160 ppt, with temperatures between the freezing points of the individual solutions and 20°C. The data from these experiments were then least-squares fitted to a power law for the conductivity and a first-order polynomial for the temperature.

Having thus obtained an expression for $\gamma(T, S)$, Equation (2) is used to calculate the liquid fraction of the forming mushy layer. The bulk salinity S_b is obtained by multiplying the liquid fraction by the local salinity of the interstitial brine S obtained from Equation (3),

$$S_b = (1 - \phi)S. \qquad (8)$$

The solid fraction ϕ, calculated from Equation (2), was used in two different ways to examine the applicability of the underlying theory. First, the solid fraction obtained from our method with two parallel wires at each level was compared with that from a measurement of the impedance between each of these two individual wires and a large carbon rod in the water at the top of the tank. The latter technique was successfully used by SHW in their laboratory experiments, but failed to give us reliable results in the field. Figure 4 shows the results from one of the comparative experiments, in which a 5.6% NaNO$_3$ solution was cooled from below to −14 °C, as in the original experiment by SHW. The figure shows the solid fraction as a function of height scaled by the ice thickness. Thus the relative position of a wire is 1 when it is first reached by the ice, and decreases steadily with growing ice thickness. The data show very good agreement between the solid fractions obtained by the two different methods, and we did not find the deviation between the two methods that was reported by Shirtcliffe and Kerr (1992). The parallel-wire method is more accurate in a field setting, where the environmental conditions of the carbon rod are not as constant as in a controlled laboratory experiment.

Secondly, the measured solid fraction for an experiment in which a 35 ppt NaCl solution was cooled from below

to −20 °C was compared with theoretical predictions of the solid fraction. For ice growing from the cooled base of the tank, no convection is expected to occur and a similarity solution for the distribution of the solid fraction within the ice can be found. The theory is described by Chiareli and others (1994) and was adjusted for our set-up by implementing the non-linear liquidus relationship (3) into the theory. A comparison of the theoretically predicted value with the measured data is shown in Figure 5, plotted in the same way as Figure 4. The figure contains data from the wire pairs at 1, 5.5 and 8 cm above the base of the tank. There is a consistent trend towards lower solid fractions at the lower wires. This deviation from the theory may be caused by a combination of significant kinetic undercooling (Kerr and others, 1990) during the fast growth of the ice in the first few hours and a slow downward movement of brine during the course of the experiment, which took around 15 hours. The kinetic undercooling and the movement of brine, which is probably caused by edge effects in the tank, where highly saline solution accumulated during the experiment, are not accounted for in the theory. SHW found no such deviation between the solid fractions at the positions of the three wires they used, because their wires were rather close together near the bottom of the tank. In our experiment we see a similar agreement of the data from the wires at the depths used by SHW. Overall, good agreement is found between the theoretical curve and the measured data, especially at depths that are only weakly influenced by the additional downward salt transport in the laboratory experiment and are only reached by the ice growing sufficiently slowly that kinetic undercooling is negligible. This indicates the utility of the assumptions which were used in interpreting the data. The comparison of data from nine laboratory experiments with theoretical predictions yields a maximum error of 15% for the measured bulk salinity. Given that this error is partly caused by the experimental set-up with kinetic undercooling and edge effects in the tank, the maximum error in the field will likely be less, and certainly is far smaller than the variation in salinity resulting from brine drainage.
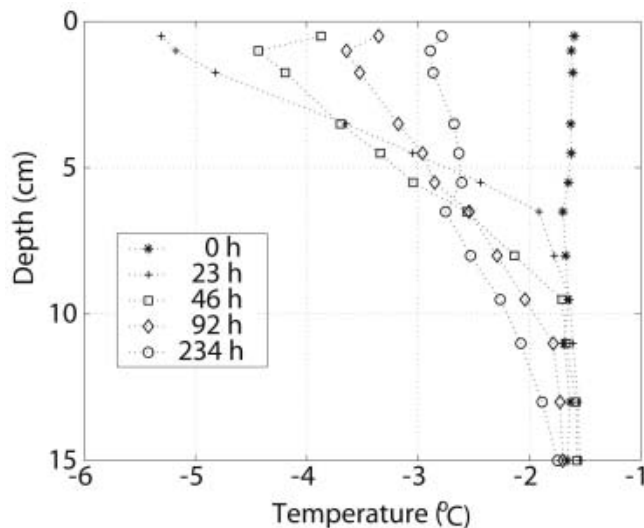
4. RESULTS FROM FIELDWORK

In March 2003, the instrument with parallel wires at each level was used in a field campaign on Adventfjord, Svalbard. The instrument was deployed in a hole approximately 1 m by 1 m that was cut out of the existing sea ice, which was about 52 cm thick. The box with the datalogger was placed downwind to minimize artificial changes in environmental conditions, especially with respect to the accumulation of snow on the measurement site during storms.

For the first 5 out of the 9 days of this experiment, the temperature and impedance at each level was sampled every 15 min with a DataTaker 800. The sampling interval was increased to 30 min for the remaining 4 days. Due to technical problems with the datalogger, which were probably caused by a failure in the power supply, the data record is not continuous but has several gaps spanning periods of 1–36 hours. As can be seen from Figure 6a, the air temperature varied between −30°C and −3°C during the course of the experiment. Strong winds (see Fig. 6b) led to the drift and accumulation of large amounts of snow at the measurement site, which significantly reduced ice growth rates.

The data were processed in the same manner as described in section 3. The solid fraction was calculated from Equation (2), and the bulk salinity from Equation (8), where the liquidus relationship for sea ice

$$S = -0.019956T^3 - 1.0015T^2 - 22.7T - 3.9921 \qquad (9)$$

is used to calculate the salinity of the interstitial brine in sea ice (Cox and Weeks, 1986), where T is in °C and S is in psu. Equation (9) has been obtained by fitting a third-order polynomial to the data presented by Assur (1958) and is valid for sea-ice temperatures of −2 to −22.9°C. At lower temperatures, solid salt crystals occur in significant amounts and different fits have to be used (Cox and Weeks, 1986).

Figure 7 shiows the temperature profiles through the ice, as measured by the calibrated thermistor string that is attached to the instrument. Figure 8 shows the temporal evolution of the solid fraction as a function of time for three different depths. The highest solid fractions (above 90%)
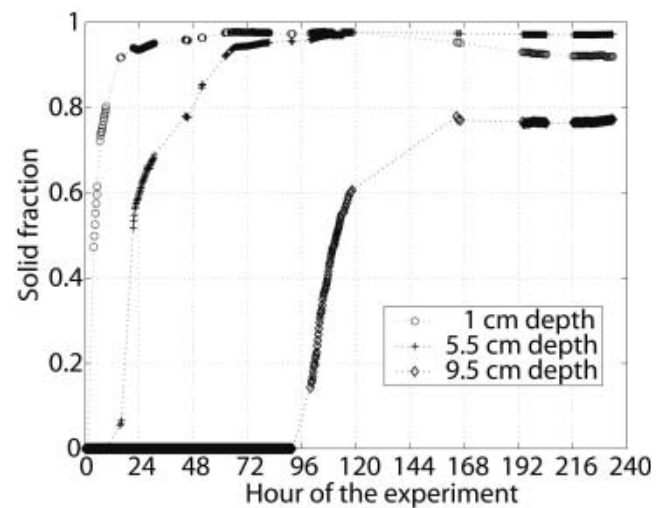
should be interpreted with care, as the impedance at this stage is too high to be properly resolved by the electronics used and the solid fraction might be underestimated. This is because we highly amplify the change in impedance in order to increase the resolution during the initial stages of sea-ice formation. This high amplification leads to a saturation of the amplifiers at high impedances. A different circuit design with different amplifications for low and high impedances should overcome this problem.

Even with these limitations, Figure 8 illustrates the high temporal resolution of the measurement, which makes it possible to analyze the rapid evolution of the solid fraction in the first hours of ice formation at a certain depth. Just before the ice–water interface reaches a wire pair, we find a systematic decrease in the measured temperature of up to 0.15°C with no significant change in the measured impedance. This might be caused by the occurrence of supercooled water, but can also simply be attributed to a thermal boundary layer ahead of the ice–water interface. The salinity measurements in the water using our instrument are too crude to allow for a conclusive interpretation of this change in temperature. The signal of the salt rejected from the ice is probably too small to change the impedance of the underlying wires noticeably, as the rejected salt would be diluted quickly in the ocean water.

Profiles of the bulk salinity at different stages of the experiment are shown in Figure 9. The instrument-derived data are compared with core-derived data from the same measurement site. Analogous to the high solid fraction, the low salinities measured by our instrument should be interpreted with care owing to the saturation of the electronics. However, especially in the later cores, there is good agreement between the two methods in the higher parts of the core, where the solid fraction is large enough to prevent the outflow of significant amounts of brine while the core is taken up. By contrast, the difference in the lower parts is clearly visible, where the bulk salinities obtained from the ice cores are consistently too small. This is due to the outflow of brine from the ice cores during recovery. The salinity profiles that were measured in situ show the
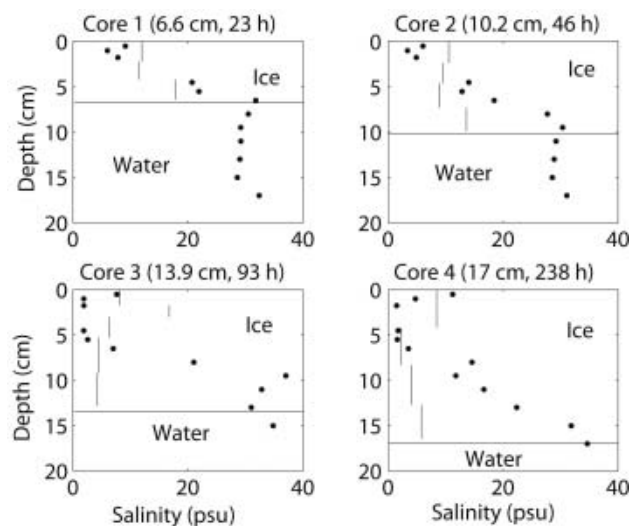
Fig. 9. Comparison of the bulk salinity as measured from ice cores (lines) and calculated from impedance measurements (dots). The horizontal line in each plot indicates the location of the ice–water interface.

Fig. 10. Mean salinity $\overline{S}$ (ppt) averaged over the 17 cm depth covered by our instrument as a function of time. Gaps in the data are due to temporary failures of power.

C-shaped profile in the salinity distribution that is typical for first-year sea ice (Cox and Weeks, 1988, and references therein). The salinity measurements obtained in water depicted in Figure 9 are not accurate, as they were derived assuming that the liquidus relationship (Equation (9)) is also satisfied in the water, which leads to an underestimate of the salinity. An independent salinity measurement in the water (e.g. by using a CTD) would help in interpreting these measurements.

By integrating the calculated salinities over the 17 cm depth covered by our instrument, it is possible to derive a time series of the total salinity content and hence to derive salt fluxes. Figure 10 shows a time series of the mean salinity obtained in our experiment. Even though the data contain too many gaps to allow for a reliable calculation of the salt flux as it evolves in time, it is interesting to note that the salt flux does not seem to be continuous, but is rather intermittent. For example, the large change in salinity which was measured just before the 48th hour of the experiment is followed by a rather constant salinity and hence diminishing salt fluxes. These fluctuations could have important implications for the interaction between growing sea ice and the structure of convection in the underlying water masses. Even though the amount of measured data is too small to permit any final conclusions about this subject, Figure 10 clearly shows the applicability of our instrument for measuring possible events of sudden brine release, as have been shown by Wettlaufer and others (2000).

Although some improvements in the system are warranted, the results presented in this section clearly show the applicability of the instrument in the field.

5. DISCUSSION

We have described an instrument which uses non-destructive impedance measurements to obtain the salinity and solid-fraction profiles within growing sea ice in situ with very high temporal and spatial resolution. The measured profiles in upward-growing sodium chloride ice in a laboratory experiment have been found to be in good
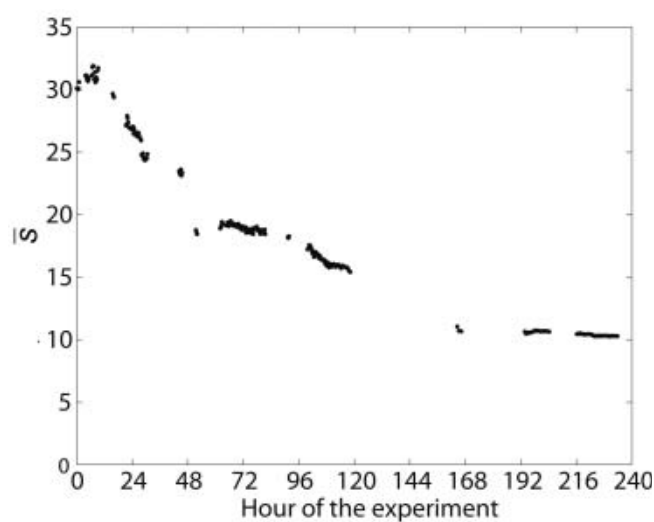
agreement with theoretical predictions. The comparison of bulk salinity profiles in growing sea ice as measured by the instrument with those measured from ice cores shows clearly that the bulk salinity in the more porous, lower part of ice cores should be interpreted with care. In ice cores this bulk salinity is significantly lower than that obtained from the in situ measurements from our instrument.

The instrument is a valuable tool both in short-term experiments with a high temporal and spatial resolution (e.g. the investigation of newly formed sea ice in leads) and in long-term experiments (e.g. the automated measurement of the change in salinity in sea ice over the course of a year). This flexibility stems from the fact that the temporal and spatial resolution of the measurement can be freely adjusted, with a single measurement at any particular depth taking <1 s. The vertical spacing between the wires can be at least as low as 5 mm without affecting the ice growth significantly, whereas with an increased spacing between the wires the instrument could be designed to measure the salinity of growing sea ice with a thickness of several meters.

The coupling of ice flow and subglacial mechanics and thermodynamics is an area of active research from field-based, laboratory and theoretical perspectives. Recently, borehole photography led to the discovery of water cavities at the base of Kamb Ice Stream (former Ice Stream C) in West Antarctica (Carsey and others, 2002), and quantitative observation of such features holds promise for improved understanding of the dynamics and thermodynamics controlling glacier–till interactions. In order to distinguish long-term variations from more abrupt phenomena (e.g. Conway and others, 2002), it is prudent to deploy an instrument capable of locating interfaces between phases at the base of glaciers or ice streams. We suggest that the concept described herein could be applied to such studies.

For laboratory use, our instrument overcomes some of the problems that Cox and Weeks (1975) mentioned in their discussion of the usage of radioactive tracers to determine the salinity of sodium chloride ice. For example, the bulk salinity throughout the whole ice layer can be measured even at very high growth rates, given that a single

measurement only takes fractions of a second compared to the 20 min per cm of ice thickness Cox and Weeks (1975) needed when using radioactive tracers.

The instrument detailed in this paper can measure the in situ evolution of the liquid and solid fractions of sea ice, and mushy layers in general, over a very large range of spatial and temporal resolution. The approach should be of value in future field campaigns on sea ice and may be easily adapted for other glaciological applications.

ACKNOWLEDGEMENTS

REFERENCES

Aagaard, K., L.K. Coachman and E.C. Carmack. 1981. On the halocline of the Arctic Ocean. *Deep-Sea Res., Ser. A,* **28**(6), 529–545.

Arcone, S.A. and R. Wills. 1986. A numerical study of dielectric measurements using single-reflection time-domain reflectometry. *J. Phys. E,* **19**(6), 448–454.

Assur, A. 1958. Composition of sea ice and its tensile strength. *In Arctic sea ice. Conference held at Easton, Maryland, February 24–27, 1958.* Washington, DC, U.S. National Academy of Sciences, 106–138. (National Research Council Publication 598.)

Atkins, P.W. 1998. *Physical chemistry.* Oxford, Oxford University Press. 997 pages.

Bard, A.J. and L.R. Faulkner. 1980. *Electrochemical methods: fundamentals and applications.* New York, Wiley. 718 pages.

Campbell, J.E. 1990. Dielectric properties and influence of conductivity in soils at one to fifty megahertz. *Soil Sci. Soc. Am. J.,* **54**(2), 332–341.

Carmack, E. 2000. Review of the Arctic Ocean's freshwater budget: sources, storage and export. *In* Lewis, E.L., E.P. Jones, P. Lemke, T.D. Prowse and P. Wadhams, *eds. The freshwater budget of the Arctic Ocean.* Dordrecht, etc., Kluwer Academic Publishers, 91–126. (NATO Science Series 2, Environmental Security.)

Carsey, F., A. Behar, A.L. Lane, V. Realmuto and H. Engelhardt. 2002. A borehole camera system for imaging the deep interior of ice sheets. *J. Glaciol.,* **48**(163), 622–628.

Chiareli, A.O.P. and M.G. Worster. 1992. On measurement and prediction of the solid fraction within mushy layers. *J. Cryst. Growth,* **125**(3–4), 487–494.

Chiareli, A.O.P., H.E. Huppert and M.G. Worster. 1994. Segregation and flow during the solidification of alloys. *J. Cryst. Growth,* **139**(1), 134–146.

Conway, H., G. Catania, C. Raymond, T. Scambos, H. Engelhardt and A. Gades. 2002. Switch of flow direction in an Antarctic ice stream. *Nature,* **419**(6906), 465–467.

Cottier, F.R., H. Eicken and P. Wadhams. 1999. Linkages between salinity and brine channel distribution in young sea ice. *J. Geophys. Res.,* **104**(C7), 15,859–15,871.

Cox, G.F.N. and W.F. Weeks. 1975. Brine drainage and initial salt entrapment in sodium chloride ice. *CRREL Res. Rep.* 345.

Cox, G.F.N. and W.F. Weeks. 1986. Changes in the salinity and porosity of sea-ice samples during shipping and storage. *J. Glaciol.,* **32**(112), 371–375.

Cox, G.F.N. and W.F. Weeks. 1988. Numerical simulations of the profile properties of undeformed first-year sea ice during the growth season. *J. Geophys. Res.,* **93**(C10), 12,449–12,460.

Daum, P.H. and D.F. Nelson. 1973. Bipolar current method for determination of solution resistance. *Anal. Chem.,* **45**(3), 463–470.

Hunter, R.J. 2001. *Foundations of colloid science.* Oxford, Oxford University Press. 806 pages.

Kerr, R.C., A.W. Woods, M.G. Worster and H.E. Hubbert. 1990. Solidification of an alloy cooled from above. Part 2. Non-equilibrium interfacial kinetics. *J. Fluid Mech.,* **217**, 331–348.

Malmgren, F. 1927. On the properties of sea ice. *In* Sverdrup, H. U., ed. *The Norwegian North Polar Expedition with the 'Maud' 1918–1925. Vol. 1a no.5.* Bergen, John Griegs Boktr, 1–67.

Morey, R.M., A. Kovacs and G.F.N. Cox. 1984. Electromagnetic properties of sea ice. *CRREL Rep.* 84-2.

Nakawo, M. and N.K. Sinha. 1981. Growth rate and salinity profile of first-year sea ice in the High Arctic. *J. Glaciol.,* **27**(96), 315–330.

Ono, N. 1975. Thermal properties of sea ice IV. *CRREL Transl.* 467. 19 pages.

Perovich, D.K. *and 8 others.* 1999. *SHEBA: snow and ice studies.* Hanover, NH, U.S. Army Corps of Engineers. Cold Regions Research and Engineering Laboratory.

Schwarzacher, W. 1959. Pack ice studies in the Arctic Ocean. *J. Geophys. Res.,* **64**(12), 2357–2367.

Schwerdtfeger, P. 1963. The thermal properties of sea ice. *J. Glaciol.,* **4**(36), 789–807.

Shirtcliffe, T.G.L. and R.C. Kerr. 1992. On the use of electrical resistance and temperature as measures of the solid fraction in a mushy layer. *J. Cryst. Growth,* **125**(3–4), 495–501.

Shirtcliffe, T.G.L., H.E. Huppert and M.G. Worster. 1991. Measurements of the solid fraction in the crystallisation of a binary melt. *J. Cryst. Growth,* **113**(3–4), 566–574.

Untersteiner, N. 1968. Natural desalination and equilibrium salinity profile of perennial sea ice. *J. Geophys. Res.,* **73**(4), 1251–1257.

Weast, R.C. 1971. *Handbook of chemistry and physics. Fifty-second edition.* Cleveland, OH, Chemical Rubber Co.

Weeks, W.F. and A. Assur. 1967. The mechanical properties of sea ice. *CRREL Monogr.* II-C3.

Weeks, W.F. and O.S. Lee. 1958. The salinity distribution in young sea ice. *Arctic,* **15**(2), 93–108.

Wettlaufer, J.S., M.G. Worster and H.E. Huppert. 2000. Solidification of leads: theory, experiment, and field observations. *J. Geophys. Res.,* **105**(C1), 1123–1134.